Intelligent Automation And Soft Computing, 2020
Copyright © 2020, TSI® Press
Vol. 26, no. 1, 27–39
https://doi.org/10.31209/2018.100000062

Model Predictive Control for Nonlinear Energy Management of a Power Split Hybrid Electric Vehicle

Dehua Shi[1,4], Shaohua Wang[2,1], Yingfeng Cai[1], Long Chen[1], ChaoChun Yuan[1], and ChunFang Yin[3]

[1]Automotive Engineering Research Institute, Jiangsu University, Zhenjiang 212013, China;
[2]School of Automobile and Traffic Engineering, Jiangsu University, Zhenjiang 212013, China;
[3] School of Electrical and Information Engineering, Jiangsu University, Zhenjiang 212013, China
[4]Jiangsu Chunlan Clean Energy Research Institute Co., Ltd., Taizhou 225300, China

ABSTRACT
Model predictive control (MPC), owing to the capability of dealing with nonlinear and constrained problems, is quite promising for optimization. Different MPC strategies are investigated to optimize HEV nonlinear energy management for better fuel economy. Based on Bellman's principle, dynamic programming is firstly used in the limited horizon to obtain optimal solutions. By considering MPC as a nonlinear programming problem, sequential quadratic programming (SQP) is used to obtain the descent directions of control variables and the current control input is further derived. To reduce computation and meet the requirements of real-time control, the nonlinear model of the system is approximated to be linear and linear time-varying (LTV) MPC strategy is studied. Simulation results demonstrate that the nonlinear MPC using SQP algorithm has best fuel economy, while the MPC using approximated linear model is superior in saving computation time.

KEYWORDS: Energy management; dynamic programming; linear time-varying mode; model predictive control; sequential quadratic programming

1 INTRODUCTION

HYBRID electric vehicles (HEVs) enable more efficient operation of the engine and energy recuperation with an additional power source. Thus, fuel consumption and exhaust emissions can be reduced (Chen, et al., 2014). Among different types of HEVs, power split HEVs make it possible that engine operation is decoupled from the vehicle motion by planetary gear sets and contributes to better fuel efficiency (Bayindir, et al., 2011). Auto-makers and scholars have designed various power split HEVs with planetary gear sets. When brakes and/or clutches are added in the planetary gear sets, the HEV will have more abundant modes for better fuel economy (Wishart, et al., 2007; Kang, et al., 2012; Miller, 2006).

In order to utilize smart HEV configurations and achieve the best possible fuel efficiency, a practicable energy management strategy is the key for power distribution within the powertrain (Taghavipour, et al., 2015). The rule-based strategy, easy to be implemented and meeting real-time requirements, has been widely used. The simple rules and maps are usually derived from engineering expertise, intuition and heuristics without a priori knowledge of the cycle (Chen, et al., 2015). Although rule-based strategy is independent of HEV model, the control parameters tuned for certain vehicles and situations may be not suitable for other situations. Another energy management strategy is model-based control scheme (Taghavipour, et al., 2015). On the basis of a control-oriented model, model-based control strategies are capable of obtaining optimal solutions by means of systematic optimizations. Global optimal power distribution calculated by dynamic programming (DP) is usually applied off-line and just used as a benchmark because of its computation burden and demand for a priori knowledge of the cycle (Yun, et al., 2015). For online application, instantaneous optimization derived from Pontryagin's minimum principle (PMP) is investigated. Another instantaneous optimization strategy is equivalent fuel consumption minimization strategy (ECMS), which is obtained.

CONTACT Shaohua Wang sjwamg@iks.edu.cn

NOMENCLATURE

A_f	vehicle frontal area	S	distance of the cycle
a_1~a_2, b_1~ b_4	fitting coefficients of engine fuel consumption	SOC	state of charge
$\boldsymbol{B_k}$	approximation to the Hessian of Lagrangian function	SOC_{ini}, SOC_{fin}	initial and final SOC
C_{d}	air drag coefficient	SOC_{lo}, SOC_{hi}	Lower and upper limit of the battery SOC
$\boldsymbol{d}$	search direction for SQP	SOC_{ref}	reference value of battery SOC
f	coefficient of rolling resistance	t_{b}	battery temperature
$f_{obj}(x)$	cost function	t_{min}	time interval for mode switching
g	gravity acceleration	T_{brk}	friction braking torque
$g_i(x)$	inequality constraints	T_{E}	torque of the engine
$h_i(x)$	equality constraints	$T_{\mathrm{E,min}}$, $T_{\mathrm{E,max}}$	minimum and maximum torque of the engine
H_{lhv}	fuel low heating value	T_{G}	output torque produced by MG1
i_{d}	ratio of the final drive	$T_{\mathrm{G,min}}$, $T_{\mathrm{G,max}}$	minimum and maximum torque of MG1
I_{C1}, I_{C2}	lumped inertia of C1, C2	T_{M}	output torque produced by MG2
I_{E}	inertia of the engine	T_{Mlim}	torque limit of MG2
I_{fd}	inertia of the main reducer	$T_{\mathrm{M,min}}$, $T_{\mathrm{M,max}}$	minimum and maximum torque of MG2
I_{G}	inertia of MG1	T_{req}	required torque at wheels
I_{M}	inertia of MG2	v_{reghi}	speed used to disable regenerative braking
I_{R1}	lumped inertia of R1	v_{thresh}	thresh speed to start engine
I_{S1}, I_{S2}	lumped inertia of S1, S2	V_{oc}	open-circuit voltage of the battery
I_w	inertia of the wheel	$\boldsymbol{Y}_{\mathrm{ref}}$	reference vector of outputs
J^*_{Np}	cost-to-go function for the Np_{th} step	α_k	update coefficient for current searching value
J^*_k	cost-to-go function for the k_{th} step	θ	road slope
K_1	characteristic parameter of PG1	ρ	penalty weight of the relaxation factor
K_2	characteristic parameter of PG2	ρ_{air}	air density
L_C	cost of the battery SOC error	P_{fuel}	fuel density
L_E	cost of the fuel consumption	η_{eng}	average efficiency of the engine
$La(\boldsymbol{x},\boldsymbol{\mu},\boldsymbol{\lambda})$	Lagrangian function	η_{ele}	average efficiency of the electric machine
$\dot{m}_f$	engine fuel consumption rate	η_{G}	efficiency of MG1
m_{fuel}	total engine fuel consumption	η_{M}	efficiency of MG2
M	total mass	ψ	map for the engine fuel flow rate
Np	prediction horizon	ω_{out}	output speed of the power coupling device
P_{bat}	battery power	ω_{E}	speed of the engine
$\boldsymbol{Q}_e$	weighing matrix for fuel consumption and SOC	$\omega_{\mathrm{E,min}}$, $\omega_{\mathrm{E,max}}$	minimum and maximum speed of the engine
Q_{bat}	battery internal capacity	ω_{G}	speed of MG1
Q_{equ}	equivalent fuel consumption of HEV	$\omega_{\mathrm{G,min}}$, $\omega_{\mathrm{G,max}}$	minimum and maximum speed of MG1
r_f	weighting factor for fuel consumption	ω_{M}	speed of MG2
r_{SOC}	weighting factor for the battery SOC	$\omega_{\mathrm{M,min}}$, $\omega_{\mathrm{M,max}}$	minimum and maximum speed of MG2
R_w	wheel radius	ε*	relaxation factor
$\boldsymbol{R}_e$	weighing matrix of control increment	Δt	time step
R_{int}	battery internal resistance	$\Delta\boldsymbol{U}$*	optimal sequence of the control increment

from heuristic by establishing the relations between electrical energy and engine fuel (Kim, et al., 2011) Nevertheless, the adaptation of predefined control parameters to other driving situations is almost impossible (Kermani, et al., 2012).

The vehicle fuel economy can be significantly improved when future driving behavior and road conditions are acquired. Especially with the development of intelligent Global Positioning/ Information System, predictable road information can contribute to better power distribution (Gong, et al., 2008; Homchaudhuri, et al., 2016). Model predictive control (MPC) is a compromise solution between global and instantaneous optimization. It is developed by incorporating future prediction information into the control-oriented model and demonstrates superior performance in dealing with nonlinear and constrained optimal problems within the limited horizon (Yang, et al., 2015; Zeng and Wang, 2015; Hiskens and Gong, 2006). The receding horizon control of MPC is to obtain the solution that minimizes the cost function which is usually described by the weighted sum of different control targets, such as fuel consumption and charge sustainability of the battery.

The optimization of HEV energy management is strongly nonlinear and constrained. Two real-time strategies were compared in (Beck, et al., 2007), where the nonlinear system dynamics was linearized and, then, the mixed integer quadratically constrained linear programming was used to reduce the computation. The continuous/GMRES algorithm was designed to realize nonlinear energy management that concerns the dynamics of battery SOC and vehicle velocity (Zhang and Shen, 2007). Yu, et al., (2015) also studied the application of continuous/GMRES algorithm. Borhan, et al. (2007) constructed two different cost functions for MPC strategy. Aiming at these cost functions, standard MPC method for linear system and optimal algorithm based on Hamilton-Jacobi-Bellman equation are utilized.

This paper investigates the application of MPC strategy in a novel power split powertrain, whose configuration is depicted in Figure 1. A buffer and locking mechanism is used to connect the engine and the carrier gear C1 of the first planetary gear set PG1, which can lock/unlock C1 and ease the rotational vibration from the engine. The electric machine MG1 is connected to S1 of PG1, while another electric machine MG2 is connected to S2 of PG2. The ring gear R2 is fixed. The carrier gear C2 is connected to the ring gear R1, and transmits the output power from different sources to the driving axle. Compound electric driving with MG1 and MG2 can be realized when the mechanism is locked. Otherwise, the power split device acts as an electric continuous variable transmission (ECVT).

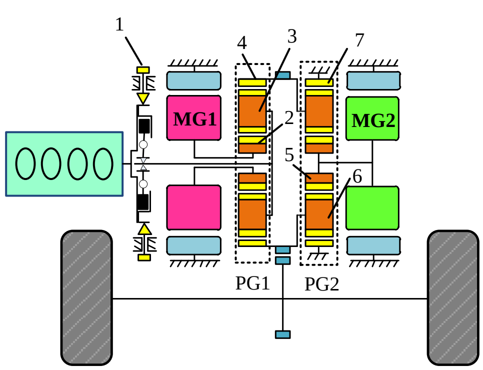

Figure 1. **Topology of power split configuration. 1-buffer and locking mechanism, 2-sun gear S1, 3-carrier gear C1, 4-ring gear R1, 5-sun gear S2, 6-carrier gear C2, 7-ring gear R2, PG1-the first planetary gear set, PG2- the second planetary gear set**

When the MPC strategy is implemented, the information access to road conditions is necessary. There are three different levels of information access to the driven route (Johannesson, et al., 2007). In this study, the highest information level, future power (torque and speed) demand, is used. Inspired by the Bellman optimal principle, DP is performed in the short horizon to obtain the optimal control sequence. Aiming at the nonlinear programming (NLP) in the receding horizon, the sequential quadratic programming (SQP) is also studied. Considering the two afore-mentioned numerical solutions are computationally demanding, the nonlinear control-oriented model is linearized for quadratic programming to increase the feasibility of real-time control.

Specifically, the rest of the paper is organized as follows. In Section 2, the system model is built. Based on hybrid automaton theory, the control frame is constructed in Section 3. Section 4 explains different algorithms for the MPC strategy, followed by simulation study in Section 5. Ultimately, Section 6 draws the conclusions.

2 SYSTEM MODELING

ACCORDING to our previous efforts (Shi, et al., 2016), the dynamic matrix equations of the system are derived by neglecting the damping and compliance. When the locking mechanism is engaged, the engine is fixed and its rotational speed is zero. The dynamic equation is

$$\begin{bmatrix} \dot{\omega}_{\mathrm{E}} \\ \dot{\omega}_{\mathrm{out}} \end{bmatrix} = \begin{bmatrix} 0 & 0 \\ 0 & \dfrac{1}{K_1^2 I_{\mathrm{gt}} + (1+K_2)^2 I_{\mathrm{mt}} + I_{\mathrm{outt}}} \end{bmatrix} \cdot \begin{bmatrix} 0 \\ (1+K_2) T_{\mathrm{M}} - K_1 T_{\mathrm{G}} - T_{\mathrm{out}} \end{bmatrix} \tag{1}$$

For the other case, the mathematical model is written as

$$\begin{bmatrix} \dot{\omega}_{\mathrm{E}} \\ \dot{\omega}_{\mathrm{out}} \end{bmatrix} = \begin{bmatrix} I_{\mathrm{gt}}(1+K_1)^2 + I_{\mathrm{et}} & -I_{\mathrm{gt}} K_1 (1+K_1) \\ I_{\mathrm{gt}}(1+K_1) + I_{\mathrm{et}} & -K_1 I_{\mathrm{gt}} + (1+K_2)^2 I_{\mathrm{mt}} + I_{\mathrm{outt}} \end{bmatrix}^{-1} \cdot \begin{bmatrix} (1+K_1) T_{\mathrm{G}} + T_{\mathrm{E}} \\ (1+K_2) T_{\mathrm{M}} + T_{\mathrm{E}} + T_{\mathrm{G}} - T_{\mathrm{out}} \end{bmatrix} \tag{2}$$

where

$$\begin{aligned} T_{\mathrm{out}} = {} & T_{\mathrm{brk}}/i_{\mathrm{d}} + \left[Mg\left(f\cos\theta + \sin\theta \right) \right] R_w / i_{\mathrm{d}} \\ & + 0.5 \rho_{\mathrm{air}} A_f C_{\mathrm{d}} \left(\omega_{\mathrm{out}} / i_{\mathrm{d}} \right)^2 R_w^3 / i_{\mathrm{d}} \end{aligned} \tag{3}$$

$$\begin{cases} I_{\mathrm{et}} = I_{\mathrm{E}} + I_{\mathrm{C1}} \\ I_{\mathrm{gt}} = I_{\mathrm{G}} + I_{\mathrm{S1}} \\ I_{\mathrm{mt}} = I_{\mathrm{M}} + I_{\mathrm{S2}} \\ I_{\mathrm{outt}} = I_{\mathrm{R1}} + I_{\mathrm{C2}} + I_{\mathrm{fd}} + \left(M R_w^2 + 4 I_w \right) / i_{\mathrm{d}}^2 \end{cases} \tag{4}$$

In the above equations, ω_{E} and ω_{out} are the speed of the engine and the output speed of the power coupling device; K_1 is the characteristic parameter of PG1, while K_2 is that of PG2, the characteristic parameter is defined by the ratio between the number of teeth of the ring gear and the sun gear; T_{G} and T_{M} are the output torques produced by MG1 and MG2; T_{E} is the torque of the engine; T_{brk} is the friction braking torque;

i_d is the ratio of the final drive; g is the gravity acceleration; θ is the road slope; f is the coefficient of rolling resistance; M is the total mass; R_w is the wheel radius; ρ_{air} is the air density; A_f is the vehicle frontal area; C_d is the air drag coefficient; I_{S1}, I_{C1} and I_{R1} are lumped inertias corresponding to S1, C1 and R1 respectively. Similar definitions are also applicable for PG2. I_E, I_G and I_M denote the inertias of different power source. I_{fd} is the inertia of the main reducer, and I_w is the wheel inertia.

The dynamics of the battery SOC are modeled as

$$S\dot{O}C=-\frac{V_{oc}(t_b,SOC)-\sqrt{V_{oc}^2(t_b,SOC)-4P_{bat}R_{int}(t_b,SOC,\lambda)}}{2Q_{bat}(t_b)R_{int}(t_b,SOC,\lambda)} \tag{5}$$

where V_{oc} is the battery open-circuit voltage, which is affected by the battery temperature t_b and SOC; R_{int} and Q_{bat} are the battery internal resistance and capacity respectively; P_{bat} is the battery power consumed by MG1 and MG2; λ denotes the following meaning

$$\lambda=\begin{cases}1 & \text{charging}\\ -1 & \text{discharging}\end{cases} \tag{6}$$

$$P_{bat}=T_M\omega_M\eta_M^{\lambda}+T_G\omega_G\eta_G^{\lambda} \tag{7}$$

where η_M and η_G are efficiencies of the motor and generator that are related to the speed and torque. Since the variation of the battery SOC and temperature in the prediction horizon is small, constant values of the battery open-circuit voltage, the battery resistance and capacity are used in each prediction horizon for the simplification of controller design.

The engine fuel consumption rate is obtained according to the quasi-static model (Sun, et al., 2015). The nonlinear relations are described as

$$\dot{m}_f=\psi(\omega_E,T_E) \tag{8}$$

where ψ is the empirical map of the engine fuel flow rate. This empirical map is difficult for controller design. Therefore, theoretical expression of the fuel flow rate with respect to the engine speed and torque is depicted by polynomial equation.

$$\dot{m}_f=(a_1\omega_E+a_2)T_E+(b_1\omega_E^3+b_2\omega_E^2+b_3\omega_E+b_4) \tag{9}$$

The coefficients of the polynomial function are obtained by fitting the map data. Figure 2 indicates the quality of the approximation. It is apparent that the explicit polynomial function can be used to calculate the fuel consumption. Meanwhile, the relation between the fuel consumption rate and the engine torque for a certain engine speed is almost linear. The coefficient of this linear function depends on the engine speed.

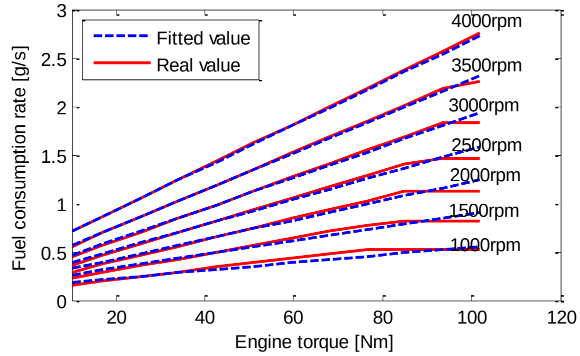

Figure 2. Approximation of the engine fuel map.

3 CONTROL SCHEME

3.1 Operation Mode

THE power split HEV can enable eight operation modes, as detailed in Table 1. The compound braking mode, where both regenerative braking and mechanical braking are applied, is included in the regenerative braking mode.

Table 1.Operation modes

Mode	Locking mechanism	Engine	MG1	MG2
MG2 driving	1/0	0	1	0/1
MG1 and MG2 driving	1	0	1	1
Hybrid driving	0	1	1	1
Engine start	0	1	1/0	1
Stop	0	0	0	0
Charging while standstill	0	1	1	0
Regenerative braking	1/0	0	1	0/1
Mechanical braking	1/0	0	0	0/1

1 represents the engine or the electric machines is on, or the mechanism is engaged, whereas 0 has the opposite meaning

Since the power of MG1 is very small when regulating the engine speed, the locking mechanism is only engaged when two electric machines cooperate to drive the HEV. It is beneficial to the controller design. As for other operation modes that the locking mechanism is disengaged, a unified control-oriented model can be selected.

3.2 Structure of the Controller

On the basis of the hybrid control scheme, the system control structure is built (Antsaklis, et al., 1993; Torrisi and Bemporad, 2004), as shown in Figure 3. The structure mainly consists of three levels, the plant level (powertrain), interface and supervisory controller. The supervisory controller describes mode transitions that are driven by a set of events obtained in the event generator. The multi-mode controller, where MPC strategy is applied to optimally distribute the power, chooses proper sub-controller according to the selected operation mode.

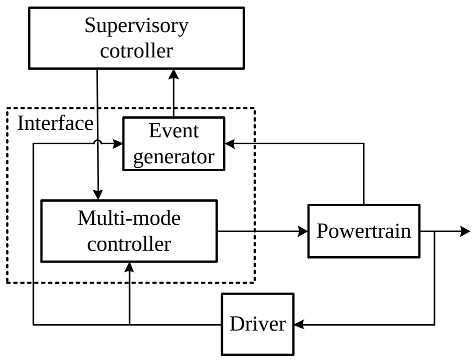

Figure 3. **Control structure.**

A finite state machine is used to model the event-driven dynamics and mode transitions in the supervisory controller. Since a unified control-oriented model is used, the operation modes are optimized and reclassified. Mode transitions in the supervisory controller are shown in Figure 4, where m_{A} denotes the set of modes when the required driving torque at the wheels is not smaller than zero, while m_{B} is the set of braking modes. Specifically, m_{A1} consists of MG2 driving mode, hybrid driving mode, stop mode, charging while standstill mode and engine start mode. m_{A2} represents the MG1 and MG2 compound driving mode. For braking situations, m_{B1} is regenerative braking mode and m_{B2} denotes the mechanical braking mode.

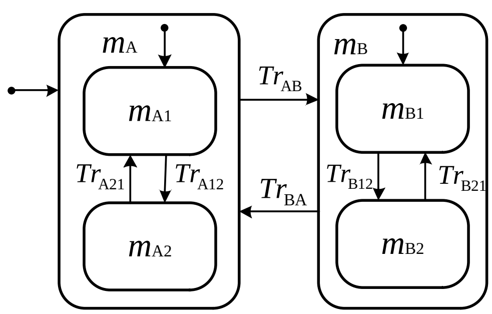

Figure 4. **Mode transitions.**

Tr means the transition between different modes. Trigger conditions of the transition are as follows:

1) Tr_{AB} and Tr_{BA} describe transitions between m_{A} and m_{B}. When the required torque T_{req} is smaller than zero, the braking mode is activated. Otherwise, the vehicle operates in mode m_{A}.

2) Tr_{A12} and Tr_{A21} are transitions in mode m_{A}. If $SOC > SOC_{lo}$ && $v > v_{thresh}$ && $T_{\mathrm{req}} > T_{\mathrm{Mlim}}$ && $t > t_{\mathrm{min}}$, the vehicle operates in mode m_{A2}. Otherwise, the vehicle is in mode m_{A1} when $T_{\mathrm{req}} \geq 0$. v_{thresh} is the vehicle speed used to decide whether the engine should be started. SOC_{lo} is the lower limit of the battery SOC and T_{Mlim} is the torque limit of MG2. The time interval t_{min} is defined to avoid frequent start/stop of the engine.

3) Tr_{B12} and Tr_{B21} denote transitions between regenerative braking mode and mechanical braking mode. When the SOC is higher than the upper boundary SOC_{hi} or the vehicle speed is larger than v_{reghi} which is defined to disable regenerative braking, the mechanical braking mode is activated. Otherwise, the vehicle operates in the regenerative braking mode.

In the multi-mode controller, control variables are set to be the engine torque and speed. The torque distribution is calculated according to the static relations within the power split device. The engine speed is regulated by MG1 through a PI controller. Details are stated in our previous study (Shi, et al., 2016).

4 ENERGY OPTIMIZATION MANAGEMENT

THE objective of the optimal energy management strategy in the study is to maximize the fuel economy with certain constraints. To maintain the battery charge sustainability, the battery SOC should also be controlled to fluctuate along the reference value. MPC strategy is explored and used in mode m_{A1} to solve the optimal power split. For mode m_{A2}, two electric machines are controlled to realize the minimum loss of electric power. In the braking mode, under the premise of safety, MG2 harvests the braking energy as much as possible.

4.1 MPC Based On Dynamic Programming

Dynamic programming (DP) can be implemented in the prediction horizon for MPC. When DP is applied off-line for a certain cycle, the initial and final battery SOC should be the same (Pisu and Rizzoni, 2007). This condition is difficult and irrational to be realized in the prediction horizon. Consequently, the final SOC at the end of the prediction horizon is controlled to be within a certain range by introducing the deviation between the actual SOC and the reference value into the cost function. The cost function is written as

$$\begin{cases} J = \min \sum_{k=0}^{Np-1} L\left(\boldsymbol{x}(k), \boldsymbol{u}(k)\right) \\ L = L_C + L_E \\ L_C\left(\boldsymbol{x}(k), \boldsymbol{u}(k)\right) = r_f\left(\dot{m}_f(k)\Delta t\right)^2 \\ L_E\left(\boldsymbol{x}(k), \boldsymbol{u}(k)\right) = r_{SOC}\left(SOC(k) - SOC_{\mathbf{ref}}\right)^2 \end{cases} \tag{10}$$

where Np is the prediction horizon; L is the cost at stage k; L_C and L_E are the cost of the battery SOC error and fuel consumption respectively; r_{SOC} and r_f are weighting factors for the battery SOC and fuel consumption; SOC_{ref} is the reference value; Δt is time step. Meanwhile, the following constraints should be enforced.

$$\begin{cases} \omega_{M,\min} \le \omega_M \le \omega_{M,\max}, & T_{M,\min} \le T_M \le T_{M,\max} \\ \omega_{G,\min} \le \omega_G \le \omega_{G,\max}, & T_{G,\min} \le T_G \le T_{G,\max} \\ \omega_{E,\min} \le \omega_E \le \omega_{E,\max}, & T_{E,\min} \le T_E \le T_{E,\max} \end{cases} \tag{11}$$

where $\omega_{M,\min}$ and $\omega_{M,\max}$ denote the minimum and maximum speed of MG2, while $T_{M,\min}$ and $T_{M,\max}$ are the minimum and maximum torque of MG2. Similar definitions are also applicable to MG1 and the engine. The range of the battery SOC are automatically decided when the SOC is discretized. The global optimization problem is converted to a series of staged optimization problems. Then, the optimal solution is obtained through reverse recursive approach.

For the Np_{th} step, the optimal cost-to-go function J^*_{Np} is

$$J^*_{Np}\left(\boldsymbol{x}(Np)\right) = 0 \tag{12}$$

For the k_{th} step ($0 \le k \le Np-1$), the optimal cost-to-go function J^*_k is written as

$$J^*_k\left(\boldsymbol{x}(k)\right) = \min_{u(k)}\left[L\left(\boldsymbol{x}(k), \boldsymbol{u}(k)\right) + J^*_{k+1}\left(\boldsymbol{x}(k+1)\right)\right] \tag{13}$$

The state variable is chosen to be the battery SOC, and the state transition equation is rewritten as

$$SOC(k+1) = SOC(k) - \frac{V_{oc} - \sqrt{V_{oc}^2 - 4P_{bat}R_{int}}}{2Q_{bat}R_{int}}\Delta t \tag{14}$$

The computation quantity of DP is closely related to the number of discrete grids. By searching along the engine optimal operation line (OOL), the number of discrete grids is greatly reduced. The OOL is shown in Figure 5.

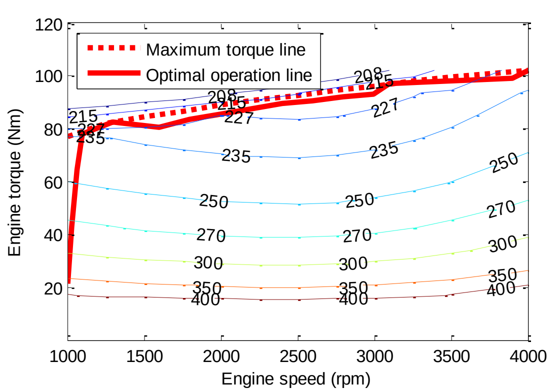

Figure 5. Engine fuel consumption map.

4.2 MPC Based On Sequential Quadratic Programming

To calculate the optimal control sequence, the nonlinear MPC can be viewed as NLP problem in the limit horizon. The generic form of the NLP problem is written as

$$\begin{aligned} J &= \min \ f_{obj}(\boldsymbol{x}) \\ \text{s.t.} \quad & h_i(\boldsymbol{x}) = 0, \ i \in E = \{1,\dots,m\} \\ & g_i(\boldsymbol{x}) \ge 0, \ i \in I = \{1,\dots,l\} \end{aligned} \tag{15}$$

where $f_{obj}(x)$ is the cost function; $h_i(\boldsymbol{x})$ and $g_i(\boldsymbol{x})$ are equality and inequality constraints. In this section, the variable $\boldsymbol{x}$ indicates the control sequence in the prediction horizon, where the control variables are the engine torque and speed. As for the HEV energy management, the cost function is still denoted by equation (10). SQP, developed from Newton-iterative method, is used to solve this NLP problem (Walther and Biegler, 2016). The values used to update the current iterative point are computed by solving the following quadratic programming problem at each iterative step.

$$\begin{aligned} J &= \min \ \frac{1}{2}\boldsymbol{d}^T\boldsymbol{B}_k\boldsymbol{d} + \nabla f_{obj}(\boldsymbol{x}_k)^T\boldsymbol{d} \\ \text{s.t.} \quad & h_i(\boldsymbol{x}_k) + \nabla h_i^T(\boldsymbol{x}_k)\boldsymbol{d} = 0, \ i \in E = \{1,\dots,m\} \\ & g_i(\boldsymbol{x}_k) + \nabla g_i^T(\boldsymbol{x}_k)\boldsymbol{d} \ge 0, \ i \in I = \{1,\dots,l\} \end{aligned} \tag{16}$$

where $\boldsymbol{d}$ is the search direction; $\nabla f(\boldsymbol{x}_k)$, $\nabla h_i(\boldsymbol{x}_k)$ and $\nabla g_i(\boldsymbol{x}_k)$ are the corresponding gradients; $\boldsymbol{B}_k$ is the approximation to the Hessian of the Lagrangian function (Shen, et al., 2015; Dang, et al., 2008).

$$\begin{cases} \boldsymbol{B}_{k+1} = \boldsymbol{B}_k - \dfrac{\boldsymbol{B}_k\boldsymbol{s}_k\boldsymbol{s}_k^T\boldsymbol{B}_k}{\boldsymbol{s}_k^T\boldsymbol{B}_k\boldsymbol{s}_k} + \dfrac{\boldsymbol{z}_k\boldsymbol{z}_k^T}{\boldsymbol{s}_k^T\boldsymbol{z}_k} \\ \boldsymbol{s}_k = \boldsymbol{x}_{k+1} - \boldsymbol{x}_k \\ \boldsymbol{y}_k = \nabla_k La(\boldsymbol{x}_{k+1}, \boldsymbol{\mu}_{k+1}, \boldsymbol{\lambda}_{k+1}) - \nabla_k La(\boldsymbol{x}_k, \boldsymbol{\mu}_{k+1}, \boldsymbol{\lambda}_{k+1}) \\ \boldsymbol{z}_k = \theta_k\boldsymbol{y}_k + (1-\theta_k)\boldsymbol{B}_k\boldsymbol{s}_k \end{cases} \tag{17}$$

where $La(\boldsymbol{x},\boldsymbol{\mu},\boldsymbol{\lambda})$ is the Lagrangian function and $\theta(k)$ is the coefficient. They are defined as

$$La(\boldsymbol{x},\boldsymbol{\mu},\boldsymbol{\lambda}) = f_{obj}(\boldsymbol{x}) - \sum_{i\in E}\mu_i h_i(\boldsymbol{x}) - \sum_{i\in I}\lambda_i g_i(\boldsymbol{x}) \tag{18}$$

$$\theta_k = \begin{cases} 1, & \boldsymbol{s}_k^T\boldsymbol{y}_k \ge 0.2\boldsymbol{s}_k^T\boldsymbol{B}_k\boldsymbol{s}_k \\ \dfrac{0.8\boldsymbol{s}_k^T\boldsymbol{B}_k\boldsymbol{s}_k}{\boldsymbol{s}_k^T\boldsymbol{B}_k\boldsymbol{s}_k - \boldsymbol{s}_k^T\boldsymbol{y}_k}, & \boldsymbol{s}_k^T\boldsymbol{y}_k < 0.2\boldsymbol{s}_k^T\boldsymbol{B}_k\boldsymbol{s}_k \end{cases} \tag{19}$$

After calculating the descent direction with SQP, optimization variables are further updated according to the iterative equation.

$$\boldsymbol{x}_{k+1} = \boldsymbol{x}_k + \alpha_k \boldsymbol{d}_k \tag{20}$$

where α_k is the update coefficient for the current searching value.

4.3 MPC Based On Linear Time Varying Model

Nonlinear MPC improves the accuracy of the optimal solutions with numerical algorithms. However, it also increases the computation complexity, especially for the nonlinear system having high orders. When the control-oriented model is linear, the nonlinear MPC problem can be converted to linear MPC problem, thus the computational burden is greatly reduced.

$$\begin{cases} \dot{\boldsymbol{x}} = f(\boldsymbol{x}, \boldsymbol{u}) \\ \boldsymbol{y} = g(\boldsymbol{x}, \boldsymbol{u}) \end{cases} \tag{21}$$

where $\boldsymbol{x}$=[SOC] and $\boldsymbol{u}$=[T_E, ω_E]^T are the state variable and control input vector; $\boldsymbol{y}$=[$\dot{m}_f$, SOC]^T is the output vector. In this section, $f(x,u)$ denotes the state transition function. The nonlinear model is linearized around the current point (x_0, u_0) using Taylor series. By ignoring high order terms and discretizing the continuous linear model, the system model is finally approximated as

$$\begin{cases} \tilde{\boldsymbol{x}}(k+1|t) = \tilde{\boldsymbol{A}}_{k,t}\tilde{\boldsymbol{x}}(k|t) + \tilde{\boldsymbol{B}}_{k,t}\Delta\boldsymbol{u}(k|t) + \tilde{\boldsymbol{d}}(k|t) \\ \boldsymbol{y}(k|t) = \tilde{\boldsymbol{C}}_{k,t}\tilde{\boldsymbol{x}}(k|t) + \tilde{\boldsymbol{D}}_{k,t}\Delta\boldsymbol{u}(k|t) + \tilde{\boldsymbol{e}}(k|t) \end{cases} \tag{22}$$

where

$$\tilde{\boldsymbol{A}}_{k,t} = \begin{bmatrix} \boldsymbol{I} + T_s\boldsymbol{A}_{k,t} & T_s\boldsymbol{B}_{k,t} \\ 0 & \boldsymbol{I} \end{bmatrix};\ \tilde{\boldsymbol{B}}_{k,t} = \begin{bmatrix} T_s\boldsymbol{B}_{k,t} \\ \boldsymbol{I} \end{bmatrix};$$

$$\tilde{\boldsymbol{C}}_{k,t} = \begin{bmatrix} \boldsymbol{C}_{k,t} & \boldsymbol{D}_{k,t} \end{bmatrix};\ \tilde{\boldsymbol{D}}_{k,t} = \boldsymbol{D}_{k,t};$$

$$\tilde{\boldsymbol{x}}(k|t) = \begin{bmatrix} \boldsymbol{x}(k|t) \\ \boldsymbol{u}(k-1|t) \end{bmatrix};\ \tilde{\boldsymbol{d}}(k|t) = \begin{bmatrix} \boldsymbol{d}(k|t) \\ 0 \end{bmatrix};$$

$$\Delta\boldsymbol{u}(k|t) = \boldsymbol{u}(k|t) - \boldsymbol{u}(k-1|t);$$

$$\tilde{\boldsymbol{d}}(k|t) = \boldsymbol{x}_0(k+1|t) - (I + T_s\boldsymbol{A}_{k,t})\boldsymbol{x}_0(k|t) - T_s\boldsymbol{B}_{k,t}\boldsymbol{u}_0(k|t);$$

$$\tilde{\boldsymbol{e}}(k|t) = g(\boldsymbol{x}_0(k|t), \boldsymbol{u}_0(k|t)) - \boldsymbol{C}_{k,t}\boldsymbol{x}_0(k|t) - \boldsymbol{D}_{k,t}\boldsymbol{u}_0(k|t)$$

T_s is the discrete time interval; $\boldsymbol{A}_{k,t}$ and $\boldsymbol{B}_{k,t}$ are Jacobian matrixes of $f(\boldsymbol{x},\boldsymbol{u})$ related to state and control variables around current values, while $\boldsymbol{C}_{k,t}$ and $\boldsymbol{D}_{k,t}$ are Jacobian matrixes of $g(\boldsymbol{x},\boldsymbol{u})$. They are described as

$$\boldsymbol{A}_{k,t} = 0;\ \boldsymbol{B}_{k,t} = \begin{bmatrix} \dfrac{\partial f}{\partial T_E} & \dfrac{\partial f}{\partial \omega_E} \end{bmatrix};\ \boldsymbol{C}_{k,t} = \begin{bmatrix} 0 & 1 \end{bmatrix}^T;$$

$$\boldsymbol{D}_{k,t} = \begin{bmatrix} a_1\omega_E + a_2 & 3b_1\omega_E^2 + 2b_2\omega_E + b_3 + a_1T_E \\ 0 & 0 \end{bmatrix};$$

and

$$f = -\frac{V_{oc} - \sqrt{V_{oc}^2 - 4\left(T_{req}v/R_w - T_E\omega_E\right)R_{int}}}{2Q_{bat}R_{int}}$$

Based on this linear model, the output vector in the prediction horizon is

$$\boldsymbol{Y}(t) = \boldsymbol{\Psi}_t\tilde{\boldsymbol{x}}(k|t) + \boldsymbol{\Theta}_t\Delta\boldsymbol{u}(t) + \boldsymbol{\Gamma}_t\boldsymbol{\Phi}(t) + \boldsymbol{\Lambda}_t(t) \tag{23}$$

Detailed descriptions of the variables in equation (23) are illustrated in the reference contributed by Harati (2011). Since the cost function is quadratic, the optimal problem can be depicted by the standard MPC (Cairano, et al., 2014). By combing the prediction equation (23), the following standard quadratic programming (QP) form with linear constraints is obtained.

$$[\Delta\boldsymbol{U}^*, \boldsymbol{\varepsilon}^*] = arg\min_{\Delta\boldsymbol{U},\boldsymbol{\varepsilon}} \frac{1}{2}\begin{bmatrix} \Delta\boldsymbol{U}(t) \\ \boldsymbol{\varepsilon} \end{bmatrix}^T \boldsymbol{H}_t \begin{bmatrix} \Delta\boldsymbol{U}(t) \\ \boldsymbol{\varepsilon} \end{bmatrix} + \boldsymbol{F}^T \begin{bmatrix} \Delta\boldsymbol{U}(t) \\ \boldsymbol{\varepsilon} \end{bmatrix} \tag{24}$$

subject to

$$\boldsymbol{G}_u\Delta\boldsymbol{U}(t) + \boldsymbol{G}_\varepsilon\boldsymbol{\varepsilon} \le \boldsymbol{W}$$

where

$$\boldsymbol{H}_t = \begin{bmatrix} 2\left(\boldsymbol{\Theta}_{tr}^T\boldsymbol{Q}_e\boldsymbol{\Theta}_{tr} + \boldsymbol{R}_e\right) & 0 \\ 0 & \rho \end{bmatrix};\ \boldsymbol{F} = \begin{bmatrix} 2\boldsymbol{\varepsilon}_{tr}^T\boldsymbol{Q}_e\boldsymbol{\Theta}_{tr} \\ 0 \end{bmatrix}$$

$$\boldsymbol{\varepsilon}_{tr} = \boldsymbol{\Psi}_{tr}\tilde{\boldsymbol{x}}(k|t) + \boldsymbol{\Gamma}_{tr}\boldsymbol{\Phi}(t) + \boldsymbol{\Lambda}_{tr}(t) - \boldsymbol{Y}_{ref}$$

$\Delta\boldsymbol{U}$* and ε* are the optimal sequence of the control increment and the relaxation factor; $\boldsymbol{Y}_{ref}$ is the reference vector of outputs; $\boldsymbol{Q}_e$ and $\boldsymbol{R}_e$ are weighing matrix; ρ is the penalty weight of the relaxation factor. This QP calculates the optimal sequence of the control increment in the prediction horizon. Only the first increment is used to derive the optimal control input.

$$\boldsymbol{u}(k|t) = \boldsymbol{u}(k-1|t) + \Delta\boldsymbol{u}^*(k|t) \tag{25}$$

5 SIMULATION AND ANALYSIS

SIMULATIONS, tested in the New European Driving Cycle (NEDC), are conducted to explore the control effects of different strategies. The velocity profile of NEDC is shown in Figure 6, which consists of four repeated Urban Driving Cycles (UDC) ECE-15 and one Extra-Urban Driving Cycle (EUDC). DP-MPC, SQP-MPC and LTV-MPC are used to represent the MPC strategies based on DP, nonlinear programming with SQP and the approximated linear time-varying (LTV) model with QP. Table 2 lists the vehicle parameters. The initial SOC and reference value are all set to be 0.55. For DP-MPC and LTV-MPC, weighing factors of the engine fuel consumption and battery SOC are 1 and 5000, while those of DP-MPC are 1 and 1000. The sampling period in the prediction horizon is 1 second.

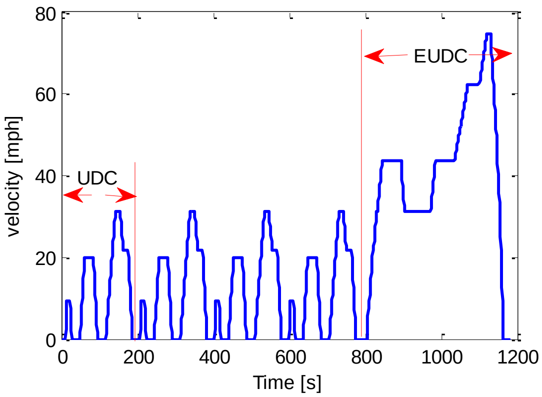

Figure 6. Velocity profile of the NEDC.

Table 2.Parameters of the HEV

Parameter	Value
Coefficient of rolling resistance f	0.008
Wheel radius R_w	0.287 m
Vehicle frontal area A_f	1.746
Air drag coefficient C_d	0.3
Air density ρ_{air}	1.23
Ratio of PG1 and PG2	2.11/2.11
Final drive ratio i_d	3.93
Engine inertia I_E	0.072 kg·m^2
Engine maximum speed ω_{E_max}	4700 rpm
Engine maximum power P_{E_max}	54 kw
MG1 inertia I_G	0.022 kg·m^2
MG1 maximum speed ω_{G_max}	8000 rpm
MG1 maximum power P_{E_max}	15 kw
MG2 inertia I_M	0.030 kg·m^2
MG2 maximum speed ω_{M_max}	15000 rpm
MG2 maximum power P_{E_max}	30 kw

As can be seen from Figures 7-9, powers of different power sources are all within their limits in the whole time history. The engine consumes fuel and provides energy to drive the vehicle, while the two electric machines either consume electrical energy or generate energy. When the vehicle speed is not high, take the UDC for example, MG2 consumes electrical energy and drives the vehicle. However, when the driving cycle is EUDC, MG2 generates electricity while MG1 consumes electrical energy. It is because that the torque of MG1 is opposite to the engine torque. When the vehicle speed is high, the speed of MG1 is also opposite to the engine speed. Consequently, MG1 consumes energy when driving the vehicle, and MG2 generates electrical energy. As shown by the power figures of MG1, the power used to adjust the engine speed is nearly zero. It is reasonable to reclassify the operation modes for the application of optimal control strategies.

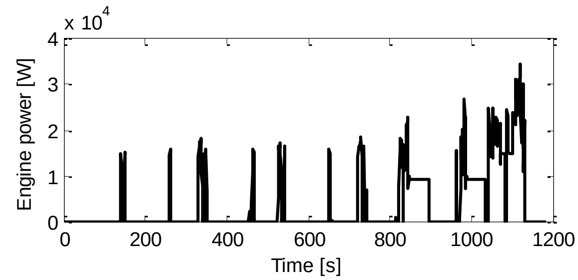

(a)

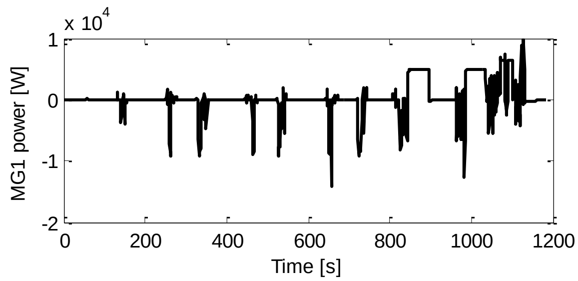

(b)

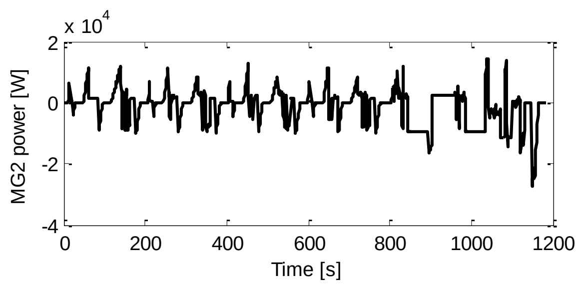

(c)

Figure 7. Simulation results with DP-MPC for NEDC: (a) power of the engine; (b) power of MG1; (c) power of MG2.

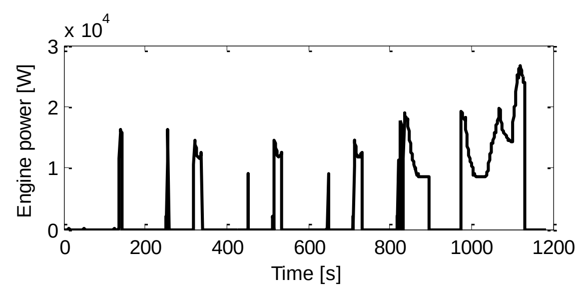

(a)

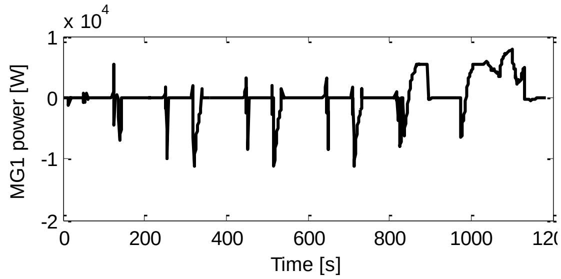

(b)

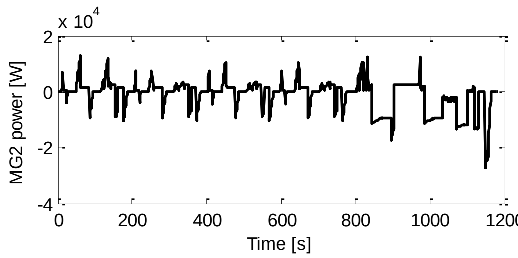

(c)

Figure 8. Simulation results with DP-MPC for NEDC: (a) power of the engine; (b) power of MG1; (c) power of MG2.

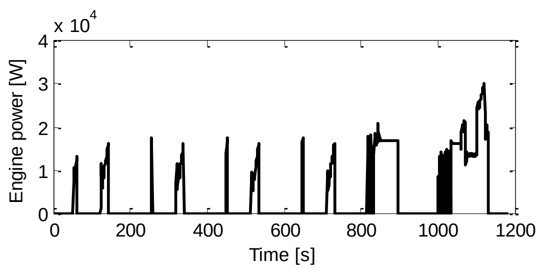

(a)

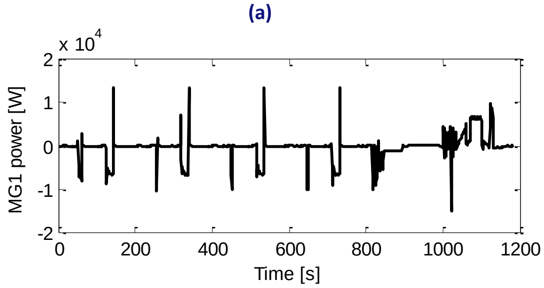

(b)

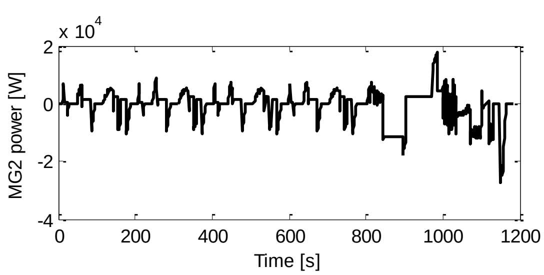

(c)

Figure 9. Simulation results with DP-MPC for NEDC: (a) power of the engine; (b) power of MG1; (c) power of MG2.

Figure 10 describes the variation of battery SOC for NEDC. It can be seen that DP-MPC and SQP-MPC strategies maintain the battery charge sustainability well. At the beginning of the first UDC, the engine operation time with LTV-MPC strategy is longer. As a result, the decline of battery SOC is not apparent. As for DP-MPC and SQP-MPC, more electrical energy at the beginning of the cycle is consumed, leading to obvious drop of battery SOC. Since the engine outputs constant larger power from 840s~900s with LTV-MPC, much of the power is used to charge the battery, resulting in the obvious increase of the battery SOC in this time region. From the point of the whole NEDC driving cycle, the battery is charged.

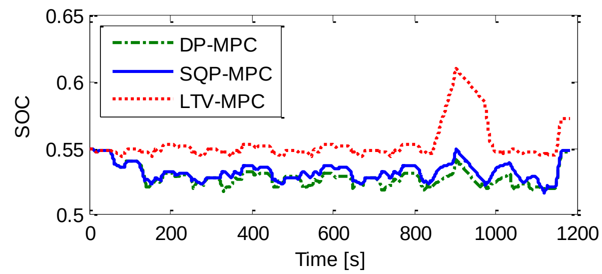

Figure 10. The battery SOC for NEDC scenario.

Figures 11 and 12 describe the engine fuel consumption and the change of the final battery SOC compared with the initial value. Fuel consumption is described by L/100km. Positive values for the variation of SOC mean that the battery is charged. Simulation results with the rule-based strategy are also given in the figures. The equivalent fuel consumption of the vehicle is given in Figure 13, where the use of electrical energy is converted to equivalent fuel consumption m_{bat}. By ignoring the variation of the battery voltage and capacity, m_{bat} is calculated by

$$m_{\mathrm{bat}} = \frac{\left(SOC_{\mathrm{ini}} - SOC_{\mathrm{fin}}\right) V_{\mathrm{oc}} Q_{\mathrm{bat}}}{H_{\mathrm{lhv}} \eta_{\mathrm{eng}} \eta_{\mathrm{ele}}} \tag{26}$$

$$Q_{\mathrm{equ}} = \frac{100\left(m_{\mathrm{fuel}} + m_{\mathrm{bat}}\right)}{S \rho_{\mathrm{fuel}}} \tag{27}$$

where SOC_{ini} and SOC_{fin} are the initial and final value of the battery SOC, respectively; H_{lhv} is the fuel low heating value; η_{eng} and η_{ele} are the average efficiencies of the engine and the electric machines; Q_{equ} is the equivalent fuel consumption of the vehicle; m_{fuel} is the total engine fuel consumption; S is the distance of the cycle; ρ_{fuel} is the fuel density.

It can be observed from Figure 11 that the engine fuel consumption is greatly reduced under the Urban Dynamometer Driving Schedule (UDDS) with rule-based strategy. However, compared with the initial value, the final SOC is reduced by 0.038, indicating that a large part of the battery electrical energy is used to drive the HEV. In terms of equivalent fuel consumption, the control effects of rule-based strategy are worse than the other three strategies, as shown in Figure 13.

The SQP-MPC strategy demonstrates best performance in maintaining the battery charge sustainability for both driving cycles. It also behaves well in reducing the equivalent fuel consumption. The DP-MPC strategy is superior in improving the HEV fuel economy for NEDC cycle. When the cycle changes, the DP-MPC strategy performs worse with the predefined control parameters. For the UDDS cycle, the DP-MPC strategy shows poor performance in maintaining the battery charge sustainability. The computation time of the DP-MPC strategy for each solving step is about 0.98s, while that of the SQP-MPC strategy is about 0.37s. It is obvious that these two strategies are difficult to be used in practice because of the computation quantity.

The reduction of engine fuel consumption with the LTV-MPC strategy is not obvious in comparison with the result of the rule-based strategy, especially for the UDDS cycle. It is because that the battery is charged with LTV-MPC and discharges with the rule-based strategy. In terms of equivalent fuel consumption, the reduction is apparent for NEDC. From Figure 12, it is obvious that LTV-MPC maintains the battery SOC worse than the other two MPC strategies. The reason is that the control effect is less sensitive to weighing factors due to the linearization of the control-oriented model. As for the computation, the time of LTV-MPC used to derive the optimal control sequence can be as little as 0.01s. If there are no convergent optimal values, the time for the solving process is about 0.04s. It can meet real-time requirements in practical applications.

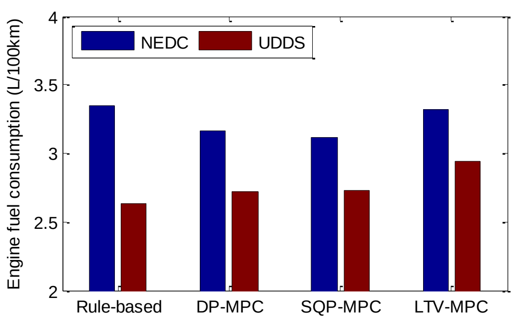

Figure 11. Engine fuel consumption.

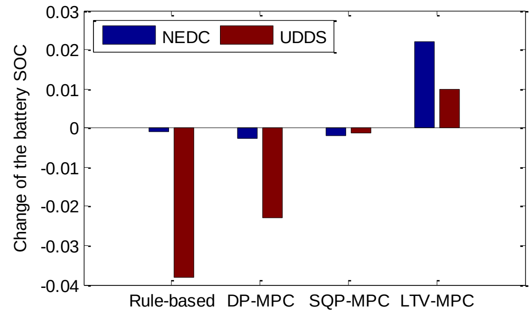

Figure 12. The change of the battery SOC.

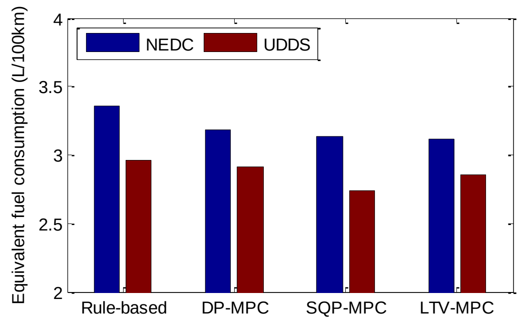

Figure 13. Equivalent fuel consumption of the vehicle.

6 CONCLUSIONS

IN the study, the MPC strategy is investigated and implemented in a dual-planetary power split HEV. Based on a hybrid control scheme, the operation modes are firstly decided according to a series of events obtained in the event generator and the MPC strategy is then applied in the multi-mode control level to split the power. In order to solve the nonlinear constrained problem of the HEV energy management, three different algorithms are investigated.

The DP and SQP algorithms are firstly explored in the limited horizon to derive the optimal solutions. To reduce the computation time, the system model is approximated to be linear, and the standard MPC problem is constructed. Simulation results demonstrate that the MPC with SQP algorithm shows significant advantages in improving fuel economy and maintaining the battery charge sustainability. Its computation time is also less than that of the DP-based MPC strategy. However, it is still difficult to put into application. LTV-MPC using approximated linear model can achieve good equivalent fuel economy. Although the control effect of LTV-MPC is not such superior to that of SQP-MPC, it can enable the minimum computational complexity. Therefore, the LTV-MPC strategy is quite promising for practical applications.

6.1 Acknowledgement

This project is funded by the National Natural Science Foundation of China (Grant No. 51475213, No. 51905219 and U1764257), the Natural Science Foundation of Jiangsu Province (No.BK20190844), the Natural Science Research Project of Jiangsu Higher Education Institutions (No.19KJB580001 and 17KJD470002) and the National Key R&D Plan (2017YFB0103200).

7 REFERENCES

P. J. Antsaklis, J. A. Stiver, and M. Lemmon, (1993). Hybrid System Modeling and Autonomous Control Systems, *Hybrid Systems Springer-Verlag*. 736, 366-392.

K. Ç. Bayindir, M. A. Gözüküçük, and A. Teke, (2011). A comprehensive overview of hybrid electric vehicle: Powertrain configurations, powertrain control techniques and electronic control units, *Energy Conversion ans Management*. 52(2), 1305-1313.

R. Beck, A. Bollig, and D. Abel, (2007). Comparison of two real-time predictive strategies for the optimal energy management of a hybrid electric vehicle, *Oil & Gas Science & Technology*. 62(4), 635-643.

H. Borhan, A. Vahidi, A. M. Phillips, M. L. Kuang, I. V. Kolmanovsky, and S. D. Cairano, (2012). MPC-based energy management of a power-split hybrid electric vehicle, *IEEE Transactions on Control Systems Technology*. 20(3), 593-603.

S. D. Cairano, D. Bernardini, A. Bemporad, and I. V. Kolmanovsky, (2014). Stochastic MPC with learning for driver-predictive vehicle control and its application to HEV energy management, *IEEE Transactions on Control Systems Technology*. 22(3), 1018-1031.

L. Chen, H. Ren, C. C. Yuan, S. H. Wang, and X. Q. Sun, (2015). Design and simulation power system for hybrid electric vehicles with wheel motors, *Journal of Jiangsu University: Natural Science Editions*. 36(1), 6-10.

Q. Chen, H. Shu, and K. Wang, (2014). Study on powertrain system for CNG-electric hybrid city bus, *Journal of Mechanical Science and Technology*. 28(10), 4283-4289.

D. Q. Dang, Y. Wang, and W. Cai, (2008). Nonlinear model predictive control (NMPC) of fixed pitch variable speed wind turbine, *IEEE International Conference on Sustainable Energy Technologies*. 29-33.

Q. Gong, Y. Li, and Z. R. Peng, (2008). Trip-based optimal power management of plug-in hybrid electric vehicles, *IEEE Transactions on Vehicular Technology*. 41(2), 4665-4670.

E. Harati, (2011). Nonlinear model predictive controller toolbox, *Chalmers University of Technology, Göteborg, Sweden*.

I. A. Hiskens and B. Gong, (2006). Voltage stability enhancement via model predictive control of load, *Intelligent Automation & Soft Computing*. 12(1), 117-124.

B. Homchaudhuri, R. Lin, and P. Pisu, (2016). Hierarchical control strategies for energy management of connected hybrid electric vehicles in urban roads, *Transportation Research Part C Emerging Technologies*.62, 70-86.

L. Johannesson, M. Asbogard, and E. Bo, (2007). Assessing the potential of predictive control for hybrid vehicle powertrains using stochastic dynamic programming, *IEEE Transactions on Intelligent Transportation Systems*. 8(1), 71-83.

J. Kang, W. Choi, and H. Kim, (2012). Development of a control strategy based on the transmission efficiency with mechanical loss for a dual mode power split-type hybrid electric vehicle, *International Journal of Automotive Technology*. 13(5), 825-833.

S. Kermani, S. Delprat, T. M. Guerra, R. Trigui, and B. Jeanneret, (2012). Predictive energy management for hybrid vehicle, *Control Engineering Practice*. 20(4), 408-420.

N. Kim, S. Cha, and H. Peng, (2011). Optimal control of hybrid electric vehicles based on Pontryagin's minimum principle, *IEEE Transactions on Control Systems Technology*. 19(5), 1279-1287.

J. M. Miller, (2006). Hybrid electric vehicle propulsion system architectures of the e-CVT type, *IEEE Transactions on Power Electronics*. 21(3), 756-767.

P. Pisu and G. Rizzoni, (2007). A comparative study of supervisory control strategies for hybrid electric vehicles, *IEEE Transactions on Control Systems Technology*. 15(3), 506-518.

G. J. Shen, S. S. Feng, and H. S. Cao, (2015). Research on a program angle optimization method for supersonic rocket target, *Acta Armamentarii*. 36(4), 644-652.

D. H. Shi, P. Pisu, L. Chen, S. H. Wang, R. C. Wang, and R. G. Wang, (2016). Control design and fuel economy investigation of power split hev with energy regeneration of suspension, *Applied Energy*. 182, 576-589.

C. Sun, X. Hu, S. J. Moura, and F. Sun, (2015). Velocity predictors for predictive energy management in hybrid electric vehicles, *IEEE Transactions on Control Systems Technology*. 23(3), 1197-1204.

A. Taghavipour, N. L. Azad, and J. Mcphee, (2015). Design and evaluation of a predictive powertrain control system for a plug-in hybrid electric vehicle to improve the fuel economy and the emissions, *Proceedings of the Institution of Mechanical Engineers Part D Journal of Automobile Engineering*. 229, 624-640.

F. D. Torrisi and A. Bemporad, (2004). HYSDEL-a tool for generating computational hybrid models for analysis and synthesis problems, *IEEE Transactions on Control Systems Technology*. 12(2), 235-249.

A. Walther and L. Biegler, (2016). On an inexact trust-region SQP-filter method for constrained nonlinear optimization, *Computational Optimization & Applications*. 63(3), 1-26.

J. D. Wishart, Leon Zhou, and Z. Dong, (2007). Review, modelling and simulation of two-mode hybrid vehicle architecture, *American Society of Mechanical Engineers*. 1091-1112.

Y. M. Yang, X. F. Lin, Z. Q. Miao, X. F. Yuan, and X. N. Wang, (2015). Predictive control strategy based on extreme learning machine for path-tracking of autonomous mobile robot, *Intelligent Automation & Soft Computing*. 21(1), 1-19.

K. Yu, H. Yang, T. Kawabe, and X. Tan, (2015). Model predictive control of a power-split hybrid electric vehicle system with slope preview, *Artificial Life & Robotics*. 20(4), 305-314.

S. Yun, K. Lee, and K. Yi, (2015). Development of a power management strategy to minimize the fuel consumption of a heavy-duty series hybrid electric vehicle, *Journal of Mechanical Science & Technology*. 29(10), 4399-4406.

J. Zhang and T. Shen, (2014). Nonlinear MPC-based power-assist scheme of internal combustion engines in plug-in hybrid electric vehicles, *In Proceedings of the European Control Conference*, Strasbourg, France. 24–27.

X. Zeng and J. Wang, (2015). A parallel hybrid electric vehicle energy management strategy using stochastic model predictive control with road grade preview, *IEEE Transactions on Control Systems Technology*. 23(6), 2416-2423.

8 DISCLOSURE STATEMENT

NO potential conflict of interest was reported by the authors

9 NOTES ON CONTRIBUTORS

Dehua Shi received the B.Sc. and Ph.D. degrees in Automotive Engineering from Jiangsu University, Zhenjiang, China, in 2011 and 2017. In 2017, he joined the Automotive Engineering Research Institute, Jiangsu University. His research interests include energy management control of hybrid electric vehicles, simulation and control of vehicle system dynamics.

Shaohua Wang received the Ph.D. degree in Automotive Engineering from Jiangsu University, Zhenjiang, China, in 2013. He is currently an associate professor with the School of Automotive and Traffic Engineering, Jiangsu University, China. His main research interests include energy management control of hybrid electric vehicles and control of electronically controlled air suspension.

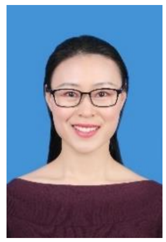

Yingfeng Cai received the B.Sc., M.Sc., and Ph.D. degrees from the School of Instrument Science and Engineering, Southeast University, Nanjing, China. She is currently a professor with the Automotive Engineering Research Institute, Jiangsu University, China. Her research interests include optimal control of hybrid electric vehicle, computer vision, intelligent transportation systems, and intelligent automobiles.

Long Chen received the Ph.D. degree in Automotive Engineering from Jiangsu University, Zhenjiang, China, in 2006. He is currently a professor with the School of Automotive and Traffic Engineering, Jiangsu University, China. He is the director of the vehicle operation key laboratory in Jiangsu Province and doctoral discipline of vehicle operation engineering. His current research interests include the areas of vehicle system dynamics and control, vehicle operation and transportation planning.

Chaochun Yuan received the Ph.D. degree in Agriculture Mechanization Engineering from Jiangsu University, Zhenjiang, China, in 2007. He is currently an associate professor with the School of Automotive and Traffic Engineering, Jiangsu University, China. His main research interests include vehicle system dynamics, control of new energy vehicles and vehicle active safety.

Chunfang Yin received the M.Sc. degree in control theory and technology engineering from Jiangsu University, Zhenjiang, China, in 2004. She is currently an associate professor with the school of electrical and information engineering, Jiangsu University, Zhenjiang, Jiangsu, China. Her research interests include vehicle system dynamics analysis and control theory research.